Research Article | Vol. 4, No. 4 / 15 April 2021 / OSA Continuum 1271

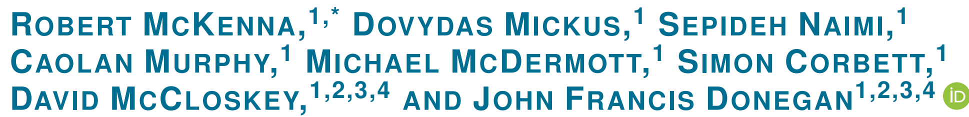

Spatially resolved self-heating and thermal impedance of laser diodes using CCD-TR imaging

ROBERT MCKENNA,[1,*] DOVYDAS MICKUS,[1] SEPIDEH NAIMI,[1] CAOLAN MURPHY,[1] MICHAEL MCDERMOTT,[1] SIMON CORBETT,[1] DAVID MCCLOSKEY,[1,2,3,4] AND JOHN FRANCIS DONEGAN[1,2,3,4]

[1] *School of Physics, Trinity College Dublin, Dublin 2, Ireland*
[2] *Future Networks and Communications (CONNECT), Trinity College Dublin, Ireland*
[3] *Centre for Research on Adaptive Nanostructures and Nanodevices (CRANN), Trinity College Dublin, Ireland*
[4] *Advanced Materials and BioEngineering Centre (AMBER), Trinity College Dublin, Ireland*
[*] *mckennr2@tcd.ie*

Abstract: The spatial distribution of the surface temperature of single and multi-section slotted semiconductor laser diodes with surface gratings is investigated experimentally with CCD-thermoreflectance imaging. The lasers are single frequency devices, operating at approximately 1550 nm. High resolution temperature maps of the laser ridge are obtained, with spatial resolution near 1 µm. The temperature profile in the direction lateral to the ridge is presented and a rapid decay in temperature away from the ridge is observed. Acquisition of the temperature maps takes about 8 minutes, with three maps required for a 400 µm device. The ridge temperature rise is shown to be linear with the power consumed by the diode. The temperature profile along the laser ridge is shown to be uniform within a section of the multi-section laser. The thermal impedance of the single section slotted laser and the various sections of the multi-section slotted laser were determined. It was found that the thermal impedance ridge length product ($Z_{th}L$) was 40 ± 6 ° C µm/mW for all section lengths. Between sections a rapid decay is also observed.

© 2021 Optical Society of America under the terms of the OSA Open Access Publishing Agreement

1. Introduction

Semiconductor lasers are currently used in a wide range of applications including optical communications, gas sensing, and as pump and seed lasers. They are complex devices that require careful design to enable optimum performance. It is well known that temperature rise from self-heating in laser diodes affects device performance and must be taken into consideration during device design and subsequent operation. The thermal impedance is an important device parameter that must be quantified and can be used in design and modelling and to characterize the expected temperature rise under operation. The thermal impedance is defined as the temperature rise due to the applied electrical power and can be given by

$$Z_{th} = \frac{\Delta T}{P_{dis}} \tag{1}$$

where ΔT is the temperature rise of the laser cavity, and P_{dis} is the electrical power dissipated as heat. The total electrical power consumed by the diode, P, is the sum of the optical power leaving the diode, P_O, and the power dissipated as heat in the diode. The dissipated power is given by

$$P_{dis} = P - P_0. \tag{2}$$

The optical power emitted by single mode semiconductor lasers is typically much lower than the dissipated power. For the devices tested in this work the wall plug efficiency is on the order of 2% [1]. As such we do not take the optical power into account in this analysis.

#422429 https://doi.org/10.1364/OSAC.422429
Journal © 2021 Received 11 Feb 2021; revised 19 Mar 2021; accepted 22 Mar 2021; published 2 Apr 2021

The first measurements of the thermal effects of a laser diode were based on measuring the laser threshold current or the spontaneous emission. [2,3] Later, Paoli developed a technique for measuring the thermal impedance using the temperature dependence of refractive index of the laser cavity. [4] This technique makes use of the lasing wavelength, which above threshold is linearly dependent on temperature, as a probe of the laser cavity temperature. This technique allows accurate determination of the laser cavity temperature for single section devices but leads to difficulties for more complex multi-section lasers. The wavelength shift is a spatially averaged property and therefore does not provide spatially resolved thermal distribution of the laser temperature. Thermal imaging is required to determine the temperature of the various sections of a multi-section laser with the sections under varying bias conditions. Infrared (IR) imaging allows a determination of a device's surface temperature, and has been used for IC devices [5]. This technique, however, has a poor spatial resolution, owing to the use of IR wavelengths in the 3–10 µm range [6]. The feature size in laser diodes can be less than 1 µm, rendering them unresolvable by IR imaging.

Thermoreflectance imaging has been developed for high resolution thermal imaging of electronic and optoelectronic devices. Thermoreflectance was first used as an imaging technique with a laser scanning configuration. [7] Later multi-pixel imaging techniques with non-CCD [8] and CCD techniques were developed [9]. CCD-TR imaging has since been utilized to obtain spatially resolved thermal profiles and to characterise a wide range of electronic and optoelectronic devices, including laser diodes [10–21]. In this work, we utilize CCD-thermoreflectance imaging to directly image the surface temperature of single and multi-section laser diodes and determine the thermal impedance of the various sections individually. These images can provide valuable information for laser design purposes. A detailed knowledge of device heating may lead to improvement in its utilization for wavelength tuning. In operation, many laser diodes use Peltier devices to control their temperature. For operation without a Peltier device, studies of the thermal profiles of the laser would be very valuable to control their operation. Our group has utilized thermal tuning to compensate for ambient temperature change allowing athermal operation over 39 ° C (continuous) and 75 ° C (discontinuous) temperature range and we presented a preliminary CCD-TR study of the devices used in this paper [1]. In athermal operation, the wavelength of the diode laser remains unchanged as its temperature is varied. Thermal imaging may also prove valuable for accelerated aging tests where hot-spots can be easily identified with high spatial resolution.

2. CCD-thermoreflectance imaging

CCD-thermoreflectance microscopy is a well-established technique for high resolution thermal imaging. This technique makes use of thermoreflectance, the dependence of the reflectance of a material on its temperature, to image the surface temperature of a sample. This dependence is quite weak, typically on the order of 1 part in 10^4, requiring advanced detection techniques. In this work, we utilize a homodyne detection technique whereby the sample is illuminated with a 530 nm CW light emitting diode and the sample is self-heated in an on-off fashion by means of current injection with a square wave of frequency *f*. The CCD camera is triggered with a signal of frequency *2f* which is phase locked to the heating signal. This has the effect of generating two images each heating cycle, a hot image and a cold image. The process is run for *N* cycles and the hot and cold images are averaged in real time. For each pixel, the temperature difference between the hot and cold images can be calculated using

$$\Delta T = \frac{I_{hot} - I_{cold}}{\kappa I_{cold}} \tag{3}$$

where I_{hot} and I_{cold} are the pixel intensities of the hot and cold images respectively, and κ is the thermoreflectance coefficient. The thermoreflectance coefficient is dependent on the illumination

OSA CONTINUUM

wavelength, the material being imaged and the numerical aperture of the objective lens of the imaging system. In this work, the material of interest is Au, which coats the upper surface of the laser diodes and provides one electrical contact to the laser. Au has been shown to have a thermoreflectance peak at 514 nm [22]. To improve the sensitivity of our system a 3 nm wide bandpass filter centred at 514.5 nm is placed below the CCD camera. Although the devices imaged in this work require high spatial resolution, they are also spatially large and a trade-off must be made between magnification and amount of image stitching required to image the entire device. We find that a 20 x magnification objective lens with a numerical aperture 0.4 provides a suitable compromise. A schematic of the setup is displayed in Fig. 2. A Thorlabs 4070M CCD camera, 530 nm Thorlabs M 530L4 LED with a maximum output power of approximately 400 mW, a GW Instek AFG-2225 Arbitrary Function Generator, and a ILX-Lightwave LDC-3220 current source were used. The heating frequency, f, and the number of frames to capture, N, are chosen to make a compromise between sensitivity and measurement time. We operate the heating current at a frequency of 12.5 Hz, resulting in an image capture rate of 25 Hz. To generate a single temperature map we capture 12,000 frames, yielding a measurement time of 480 seconds.

In order to measure absolute temperature the thermoreflectance coefficient, κ, must be accurately determined. To calibrate the system a thin Au stripe structure, 20 µm in width and 50 nm in thickness, was fabricated on a quartz substrate, a diagram of which is shown in Fig. 1(c). The calibration sample includes four contact pads to allow current injection and voltage measurement across the stripe. It has been shown by de Vries, using films ranging from 18 nm to 82 nm in thickness, that the temperature dependence of the resistivity of thin Au films is independent of sample thickness and is equal to its bulk value, and so can be utilised as a temperature probe [23]. By rearranging Eq. (3) and comparing the resistivity derived temperature rise to the relative change in pixel intensity the thermoreflectance coefficient is determined. Here, using a 20 x magnification objective lens with a NA of 0.4, we obtain a value of -1.4×10^{-4} K^{-1}.

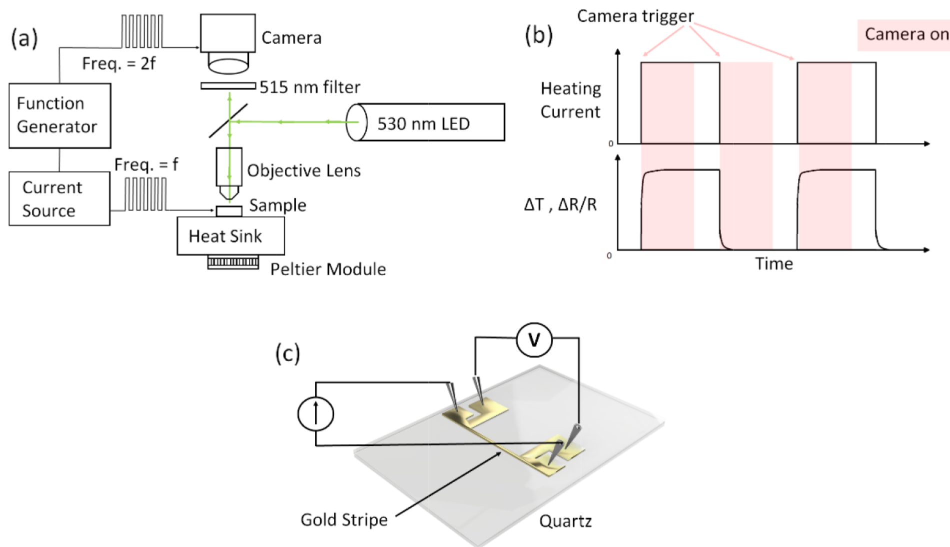

Fig. 1. (a) Schematic of the CCD-TR setup. Laser operates at frequency f and camera at 2f. (b) Representation of the CCD-TR timing sequence. (c) Representation of the gold stripe calibration sample.

OSA CONTINUUM

3. Single section slotted laser diode

Here we investigate a single mode single frequency laser diode operating at 1545 nm, shown in Fig. 2(a) and (b). Optical confinement is provided by a 2 μm wide and 1.85 μm tall ridge along the length of the device. The ridge is situated in a 24 μm wide trench. The lasers contain a high-order slotted grating, wherein 24 rectangular slots 1.3 μm in depth are etched into the surface of the ridge. The slots act as a Bragg reflector allowing selection of a single cavity mode, enabling single frequency operation with a high side mode suppression ratio (SMSR). High order surface gratings avoid the need for epitaxial re-growth, and allow large slot feature sizes for current injection into the grating region, enabling simple fabrication with high yield. The use of high order gratings allow optical gain all along the length of the device, which is provided by 5 AlGaInAs quantum wells positioned below the ridge. Figure 2(c) shows the lasing spectrum of the device operating with a 150 mA CW bias and with the heatsink maintained at 20 ° C. SMSR of 42 dB is obtained. An LIV plot of this device is shown in Fig. 2(d), again with the heatsink maintained at 20 ° C. A threshold current of 50 mA is observed. Here, the device facets are left uncoated and the waveguide is angled at 7 ° at the front of the device in order to minimize reflections from the front facet back into the waveguide.

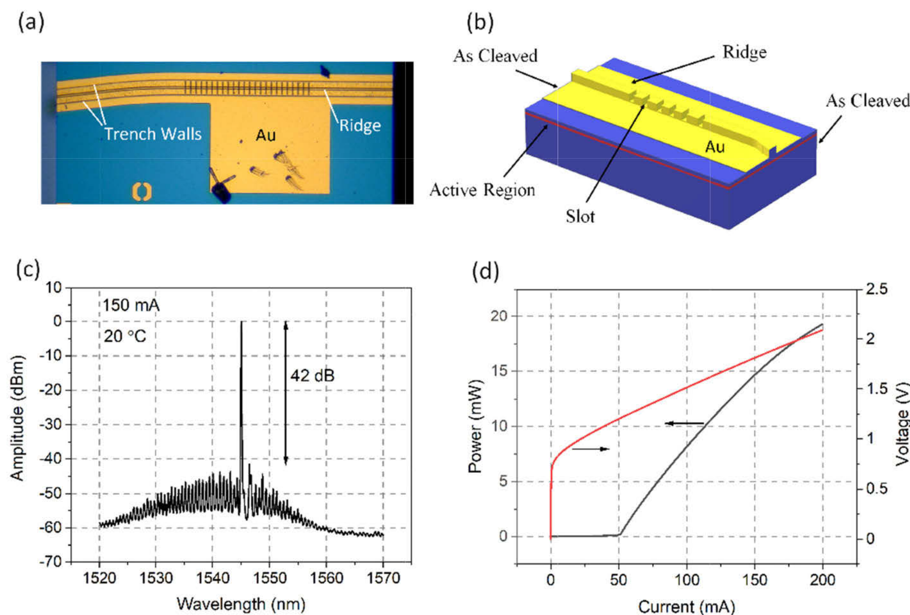

Fig. 2. (a) Optical microscope image of the single section slotted laser. Marks on Au contact pad are minor damage due to probes. (b) 3D representation of the laser. (c) Lasing spectra and (d) LIV of the single section slotted laser.

Figure 3(a) displays a composite image of the surface temperature of a single section laser diode under a 250 mA bias current as measured by the CCD-TR technique. The overall image is composed of three images stitched together. The region close to the ridge is where the temperature is highest. The short vertical lines seen midway along the ridge indicate the positions of the slots that form the high-order grating. These lines extend far beyond the ridge and result from the fabrication process. In the overall image, the region which is clearly outlined by the dashed white line is where Au has been deposited. Outside this region the temperature measurement is not valid as the thermoreflectance coefficient is different. Figures 3(b) and (d) show close ups of the temperature maps of the laser ridge and the slotted region respectively. Conventional microscope images of the same regions are shown in (c) and (e). The dashed white lined in (b-e) show the

OSA CONTINUUM

location of the ridge. These images show that that it is possible to resolve the temperature close to the ridge, however they also highlight the difficulty of interpreting the image data in the vicinity of height steps such as the ridge walls and trench walls. Vibrations during the measurement can cause pixels near vertical steps to experience changes in intensity that dominate over the thermoreflectance effect leading to nonvalid temperature readings. The small dots visible in both the thermal and topology images are slight imperfections in the Au.

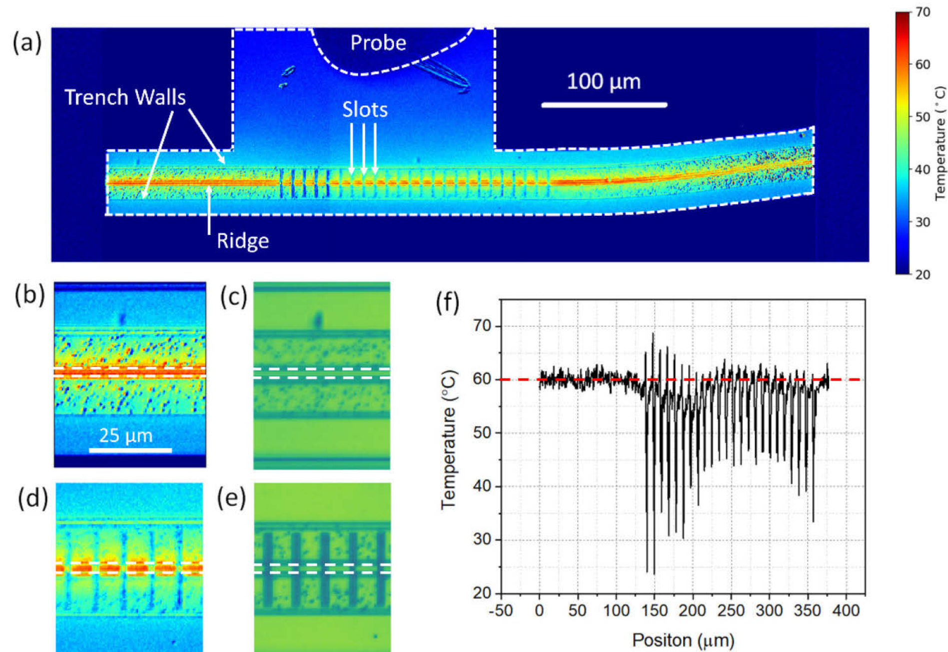

Fig. 3. (a) Temperature map of a single section slotted laser diode biased at 250 mA composed of three images stitched together. Close in of temperature of (b) the ridge and (d) the slots in (a). Microscope image of (c) the ridge and (e) the slots. In (b-e) the dashed white lines indicate the position of the ridge. (f) Profile of the temperature on the top of the ridge along the length of the waveguide. 0 position is at the left hand start of the waveguide.

Figure 3(f) shows the temperature at the top of the ridge along the length of the device from the back facet to end of the grating. The mean temperature is found to be 60 ° C as indicated by the dashed red line. In the unslotted part of the profile, a fluctuation of about 2 ° C can be observed. The fluctuation is due to spatial variations which can be greatly reduced by averaging over an area. However, here we are interested in the ridge temperature, and averaging laterally is not possible as the ridge covers only 2 to 3 pixels on the CCD array. Even still, we have chosen a 20 x lens as the use of a higher magnification lens leads to practical problems of fitting the contact probes to operate the laser below the objective lens and also requires more images to cover the entire device. In the slotted region, large variations in the temperature profile are observed. These are artefacts of the measurement system due to the presence of the slots, not valid temperature measurements. The vertical step at the slot edge results in a large change in signal.

Figure 4 shows the laser temperature under a variety of bias conditions from 100 mA to 250 mA. The temperature profiles along the non-slotted part of the laser ridge for all bias currents shown in Fig. 4 are shown in Fig. 5(a). It is clear from these profiles that the temperature does not vary significantly along the length of the waveguide shown. Figure 5(b) shows the ridge temperature averaged over the non-slotted region of the laser diode as a function of electrical power dissipated in the laser. A linear relationship is observed, as is expected from theory. The

OSA CONTINUUM

slope gives the thermal impedance, which is 74 ° C / W, close to the 75 ° C / W the value found by Mathews et. al. for similar devices [24]. It is desirable to compare the thermal impedance of lasers of various lengths. Keeping the ridge height and width constant we expect that the thermal resistance is inversely proportional to length. Thus, it is the product of the thermal impedance and the length, $Z_{th}L$ that is the parameter of relevance. For this device the current is biased over a ridge that is 550 μm in length, leading to $Z_{th}L$ = 40.7 ° C μm / mW.

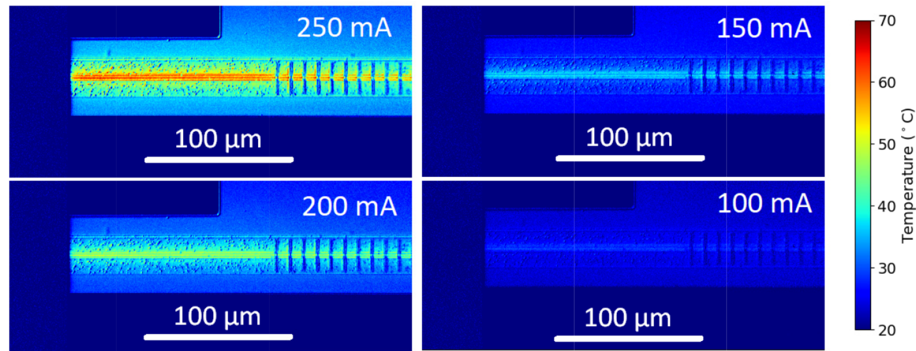

Fig. 4. Temperature maps of a part of the single section laser under a number of bias currents. The heatsink is maintained at 20 ° C of all images.

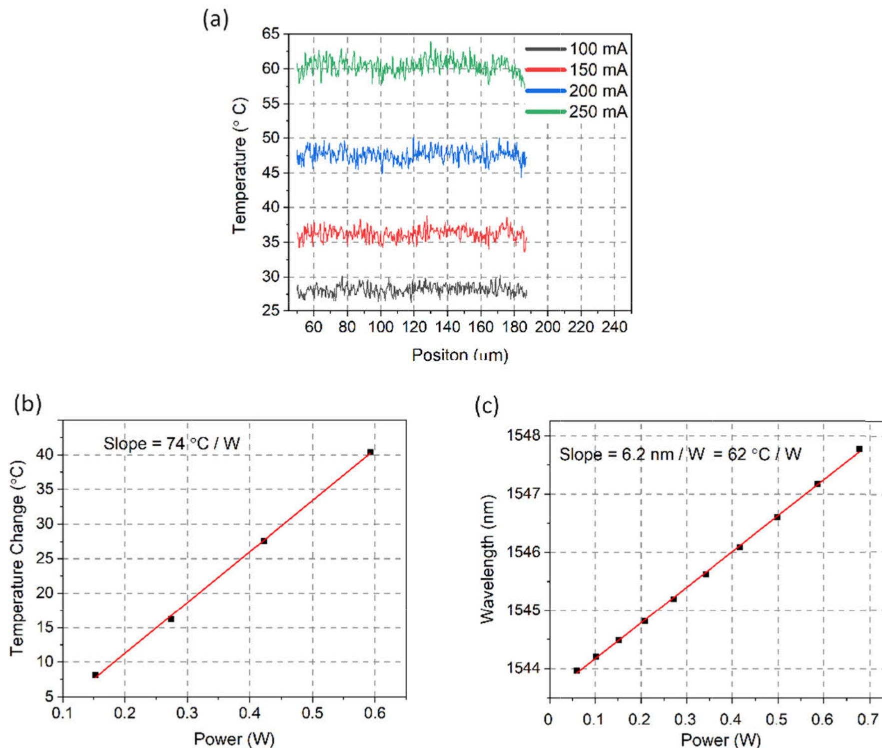

Fig. 5. (a) Temperature profiles along the non-slotted region of the single section laser under a number of bias currents with the heatsink maintained at 20 ° C. (b) Mean temperature change from ambient calculated from the profiles in (a) against the power consumption of the device. (c) Wavelength drift of the laser as the power consumption is varied.

The thermal impedance of the single section laser was also determined using the method developed by Paoli et al. [4]. Figure 5(c) shows the laser wavelength drift with electrical power giving a slope of 6.2 nm / W. Taking into account the wavelength drift with temperature which was measured to be 0.1 nm/ ° C, this implies a thermal impedance of 62 ° C/W, which is 84% of the thermal impedance as measured by thermoreflectance. The authors expect such a disparity between these two techniques as the thermoreflectance technique measures the temperature at the surface of the ridge and Paoli's technique measures the wavelength drift of the optical mode, which is largely confined to the active region 2 µm below the top of the ridge. An experimental study by Kuntze et. al. shows that the contact resistance at the p+ to p heterojunction can cause significant power consumption, and thus self-heating, local to the ridge [25]. The difference between these two measurement techniques may enable a determination of the heating in these layers.

4. Multi-section slotted laser diode

We also investigate a multi-section slotted laser diode. The device structure is identical to that of the single section laser with the exception that the top contact is segmented into three sections. This, with the addition of an isolation slot between each section, ensures electrical isolation between the sections and allows for independent biasing. Figure 6(a) shows a microscope image of the three section laser. The laser consists of a gain section, a grating section and an amplifier (SOA) section, which are 178, 194 and 190 µm in length respectively. As with the single section laser the grating provides wavelength selective feedback to ensure single frequency operation. The grating section provides enough reflection to create an optical cavity, which allows the remainder of the waveguide to be utilized as an SOA. Antireflection coating and a 7 ° bend are employed to minimize feedback from the SOA into the laser cavity. Theoretical and numerical analysis of slotted surface gratings can be found in [26–28]. Experimental characterisation of similar fabricated devices can be found in [1,29–32]. The independent tuning of the laser sections allows us to deal with mode hops which occur in these DBR-type lasers. The SOA sections can be independently biased to boost the power output.

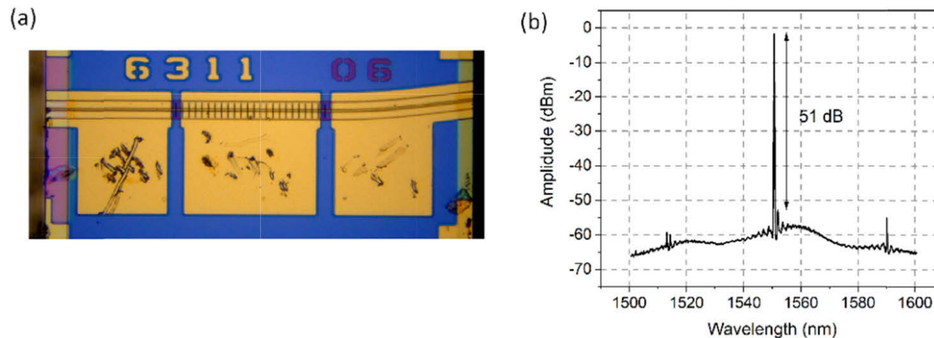

Fig. 6. (a) Optical microscope image of the multi-section slotted laser showing the gain, grating and SOA sections from left to right. (b) Lasing spectra of the laser with 80 mA gain bias current, 80 mA grating bias current and 20 mA SOA bias current. The peaks at 1512 nm and 1590 nm are due to the adjacent FSR modes for the high-order grating.

Figure 7 displays the temperature map of the three section laser as outlined in section 2 with the three sections biased independently. The thermal impedance of each section can be determined independently, as is show in Fig. 8. These are 247 ° C/W for the gain section, 179 ° C/W for the grating section and 220 ° C/W for the SOA sections. These values are considerably higher than for the single section laser as the length of waveguide is considerably shorter. Considering

the lengths of the sections the thermal impedance length product, $Z_{th}L$, is 44.0 ° C µm / mW for the gain section, 34.7 ° C µm / mW for the grating section, and 41.6 ° C µm / mW for the SOA section, reasonably close to the single section value of 40.7 ° C µm / mW. The maps in Fig. 7 also show reasonable thermal isolation between the sections. This is further shown in Fig. 9, wherein the temperature profile along the ridge is plotted with only one section biased. A small temperature rise penetrates into the adjacent section, however this rapidly decays as the distance from the biased section is increased. The shaded regions in Fig. 9 indicate the isolation region between the gain and grating contacts. This region is not contacted with Au and thus does not provide any temperature information. It is noteworthy that the temperature on the ridge can exceed 120 °C, far above the 20 °C of the Peltier.

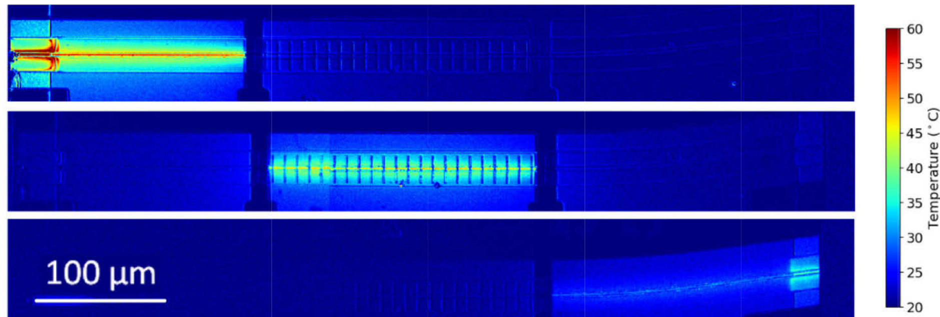

Fig. 7. Temperature map of a three section laser with (top) 80 mA applied to the gain section, (middle) 80 mA to the grating section and (bottom) 40 mA applied to the SOA section. Slight temperature rises are seen in the adjacent sections.

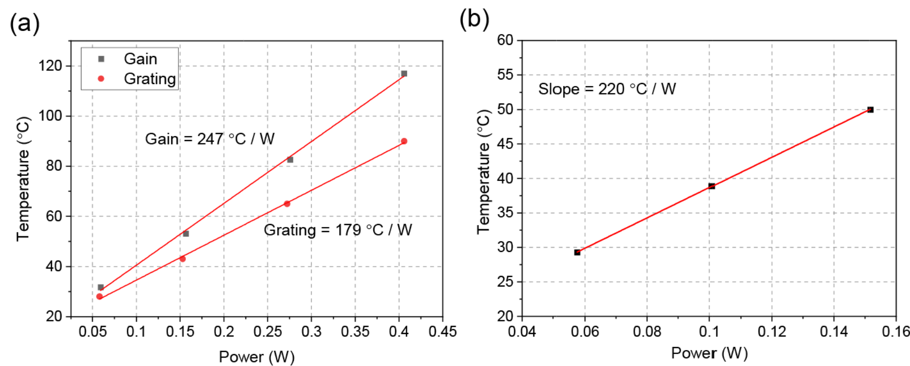

Fig. 8. Average ridge temperature vs power consumption from the (a) gain and grating sections, and (b) SOA section of the three section device.

The black curve in Fig. 10(a) shows the temperature profile in the direction lateral to the ridge of the gain section of the multi-section laser biased at 80 mA. Figure 10(b) shows the same profile viewed closer to the ridge. In both figures, the red curve above the temperature profile shows the pixel intensity of the hot image scaled to fit onto the plot. This allows easy identification of the ridge and regions of invalid temperature reading due to the presence of vertical steps which are shaded grey. It is clear that the surface temperature reaches a maximum at the ridge and rapidly decays moving away from the ridge. We approximate the temperature decay as single exponential shown by the blue curve in Fig. 10(a). The equation of fit is given by

$$T = Ae^{-x/\tau} + T_0 \quad (4)$$

OSA CONTINUUM

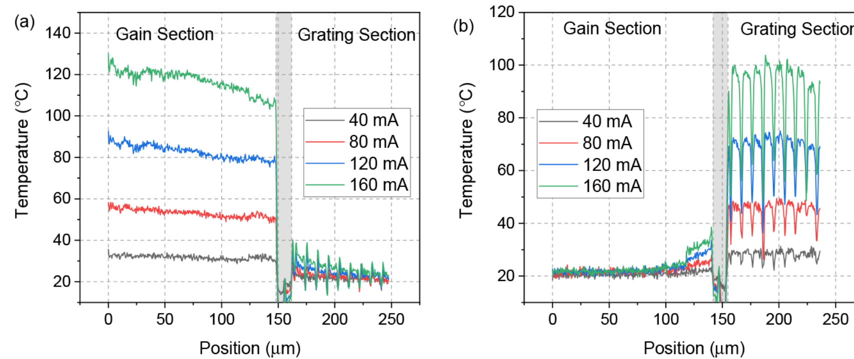

Fig. 9. Profile of the temperature change over ambient along the ridge for (a) the gain section biased and the grating unbiased and (b) the grating section biased and the gain section unbiased. The shaded region is the isolation region and is not covered with Au, thus temperature measurements here are not valid. Weak heating is again observed in the non-biased sections.

where T is the temperature, x is the distance from the ridge and τ is the decay constant, which is found to be 14.9 μm^{-1}. The amplitude, A is 20.7 ° C and T_0 is 25.1 ° C. As would be expected, T_0 is slightly higher than the 20 °C set on the TEC.

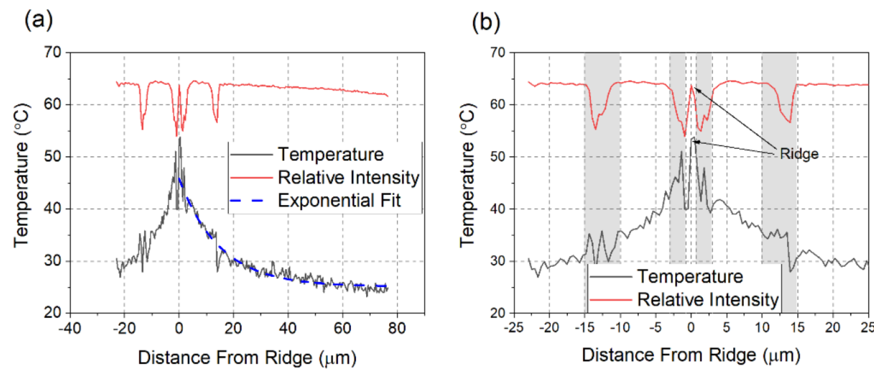

Fig. 10. Temperature Profile in the direction lateral to the ridge of the gain section biased at 80 mA. The black curve is the temperature profile. The blue curve is an exponential decay fit. The red curve shows the relative intensity of the microscope image, allowing clear identification of the ridge. (a) Wide view. (b) Profile close to ridge.

5. Conclusion

We have utilized CCD-thermoreflectance imaging to determine the spatial distribution of the surface temperature of a number semiconductor laser diodes under current injection. The technique allows high resolution imaging of the device, easily enabling determination of the temperature of the 2 μm wide laser ridge. We have determined the thermal impedance of the devices using both the thermoreflectance and the conventional mode tracking techniques. The difference between the two techniques may elucidate a method to determine the heating local to the upper layers of the ridge. We have applied the thermoreflectance technique to a multi-section semiconductor lasers and have determined the thermal impedance of each section independently, which is not possible with the conventional technique. We have demonstrated the degree of heating in adjacent sections of the laser and determined that it is minimal for all but the highest

OSA CONTINUUM

injection current densities. The technique can be used to inform thermal models of semiconductor lasers and to measure temperature profiles on a large variety of semiconductor lasers. The technique should gain wide use in the characterization of semiconductor lasers.

Funding. Science Foundation Ireland (15/IA/2854).

Disclosures. The authors declare no conflict of interest.

References

1. M. J. Wallace, R. O'Reilly Meehan, R. Enright, F. Bello, D. McCloskey, B. Barabadi, E. N. Wang, and J. F. Donegan, "Athermal operation of multi-section slotted tunable lasers," Opt. Express **25**(13), 14414 (2017).
2. C. Gooch, "The thermal properties of gallium arsenide laser structures," IEEE J. Quantum Electron. **4**(4), 140–143 (1968).
3. H. Meixner and R. Unger, "Optical Method for Determination of the Thermal Resistivity of Laser Diodes," Siemens Forsch Entwicklungsber, Res. Dev. Rep. **3**(3), 190–194 (1974).
4. T. Paoli, "A new technique for measuring the thermal impedance of junction lasers," IEEE J. Quantum Electron. **11**(7), 498–503 (1975).
5. J. Brown, P. K. Footner, and B. P. Richards, "Failure analysis of plastic encapsulated components—the advantages of IR microscopy*," J. Microsc. **148**(2), 179–194 (1987).
6. J. Christofferson, K. Maize, Y. Ezzahri, J. Shabani, X. Wang, and A. Shakouri, "Microscale and Nanoscale Thermal Characterization Techniques," in *2007 International Conference on Thermal Issues in Emerging Technologies: Theory and Application* (2007), pp. 3–9.
7. D. Guidotti and H. M. van Driel, "Spatially resolved defect mapping in semiconductors using laser-modulated thermoreflectance," Appl. Phys. Lett. **47**(12), 1336–1338 (1985).
8. J. Christofferson and A. Shakouri, "Thermoreflectance based thermal microscope," Rev. Sci. Instrum. **76**(2), 024903 (2005).
9. S. Grauby, B. C. Forget, S. Holé, and D. Fournier, "High resolution photothermal imaging of high frequency phenomena using a visible charge coupled device camera associated with a multichannel lock-in scheme," Rev. Sci. Instrum. **70**(9), 3603–3608 (1999).
10. P. Kozodoy, T. Strand, Y. Akulova, G. Fish, C. Schow, Ping Koh, Zhixi Bian, J. Christofferson, and A. Shakouri, "Thermal effects in monolithically integrated tunable laser transmitters," in *Twentieth Annual IEEE Semiconductor Thermal Measurement and Management Symposium (IEEE Cat. No.04CH37545)* (IEEE, 2004), pp. 177–183.
11. D. Luerssen, R. J. Ram, and J. A. Hudgings, "2-D thermal imaging of the optical power distribution in photonic integrated circuits," in *The 17th Annual Meeting of the IEEELasers and Electro-Optics Society, 2004. LEOS 2004.* (IEEE, 2004), 1, pp. 163–164.
12. M. Farzaneh, D. Luerben, and J. A. Hudgings, "Thermal profiling of photonic integrated circuits by thermoreflectance microscopy," in *2006 Conference on Lasers and Electro-Optics and 2006 Quantum Electronics and Laser Science Conference* (IEEE, 2006), pp. 1–2.
13. K. J. Greenberg, J. A. Summers, M. Farzaneh, and J. A. Hudgings, "Spatially-resolved thermal coupling in VCSEL arrays using thermoreflectance microscopy," in *2008 Conference on Lasers and Electro-Optics* (IEEE, 2008), pp. 1–2.
14. J. A. Summers, M. Farzaneh, R. J. Ram, and J. A. Hudgings, "Thermal and Optical Characterization of Photonic Integrated Circuits by Thermoreflectance Microscopy," IEEE J. Quantum Electron. **46**(1), 3–10 (2010).
15. C. Li, K. P. Pipe, C. Cao, P. Thiagarajan, R. J. Deri, and P. O. Leisher, "Thermal imaging of high power diode lasers subject to back-irradiance," Appl. Phys. Lett. **112**(10), 101101 (2018).
16. S. Wang, C. Xu, F. Duan, B. Wen, S. M. S. Rassel, Z. Wasilewski, L. Wei, and D. Ban, "Time-Resolved Thermoreflectance Imaging for Mid-Infrared Quantum Cascade Laser," in *2020 Conference on Lasers and Electro-Optics (CLEO)* (2020), pp. 1–2.
17. D. Pierścińska, K. Pierściński, M. Morawiec, P. Karbownik, P. Gutowski, and M. Bugajski, "CCD thermoreflectance spectroscopy as a tool for thermal characterization of quantum cascade lasers," Semicond. Sci. Technol. **31**(11), 115006 (2016).
18. D. Pierścińska, Ł. Marona, K. Pierściński, P. Wiśniewski, P. Perlin, and M. Bugajski, "High-resolution mirror temperature mapping in GaN-based diode lasers by thermoreflectance spectroscopy," Jpn. J. Appl. Phys. **56**(2), 020302 (2017).
19. D. Pierścińska, "Thermoreflectance spectroscopy—Analysis of thermal processes in semiconductor lasers," J. Phys. D: Appl. Phys. **51**(1), 013001 (2018).
20. K. P. Pipe, A. K. Jha, C. Li, M. T. Crowley, D. B. Fullager, J. D. Helmrich, P. Thiagarajan, R. J. Deri, E. Feigenbaum, R. B. Swertfeger, and P. O. Leisher, "Applications of thermoreflectance imaging to high-power diode laser diagnostics," in *2019 IEEE High Power Diode Lasers and Systems Conference (HPD)* (2019), pp. 43–44.
21. S. Wang, C. Xu, F. Duan, B. Wen, S. M. S. Rassel, M. C. Tam, Z. Wasilewski, L. Wei, and D. Ban, "Thermal dynamic imaging of mid-infrared quantum cascade lasers with high temporal–spatial resolution," J. Appl. Phys. **128**(8), 083106 (2020).
22. T. Favaloro, J.-H. Bahk, and A. Shakouri, "Characterization of the temperature dependence of the thermoreflectance coefficient for conductive thin films," Rev. Sci. Instrum. **86**(2), 024903 (2015).

OSA CONTINUUM

23. J. W. C. de Vries, "Temperature-dependent resistivity measurements on polycrystalline SiO2-covered thin gold films," Thin Solid Films **150**(2-3), 201–208 (1987).
24. I. Mathews, A. Abdullaev, S. Lei, R. Enright, M. J. Wallace, and J. F. Donegan, "Reducing thermal crosstalk in ten-channel tunable slotted-laser arrays," Opt. Express **23**(18), 23380 (2015).
25. S. B. Kuntze, E. H. Sargent, J. K. White, K. Hinzer, S. J. Dixon-Warren, and D. Ban, "*In situ* resistance measurement of the p-type contact in InP–InGaAsP coolerless ridge waveguide lasers," Appl. Phys. Lett. **86**(8), 081111 (2005).
26. Q. Y. Lu, W. H. Guo, R. Phelan, D. Byrne, J. F. Donegan, P. Lambkin, and B. Corbett, "Analysis of Slot Characteristics in Slotted Single-Mode Semiconductor Lasers Using the 2-D Scattering Matrix Method," IEEE Photonics Technol. Lett. **18**(24), 2605–2607 (2006).
27. Q. Lu, W.-H. Guo, D. Byrne, and J. F. Donegan, "Design of Slotted Single-Mode Lasers Suitable for Photonic Integration," IEEE Photonics Technol. Lett. **22**(11), 787–789 (2010).
28. F. Bello, A. Abdullaev, M. Wallace, M. Nawrocka, Q. Lu, W. Guo, and J. F. Donegan, "Traveling Wave Analysis for a High-Order Grating, Partially Slotted Laser," IEEE J. Quantum Electron. **51**(11), 1–5 (2015).
29. Q. Lu, W. Guo, M. Nawrocka, A. Abdullaev, C. Daunt, J. O'Callaghan, M. Lynch, V. Weldon, F. Peters, and J. F. Donegan, "Single mode lasers based on slots suitable for photonic integration," Opt. Express **19**(26), B140 (2011).
30. Q. Lu, W. Guo, A. Abdullaev, M. Nawrocka, T. N. Huynh, J. O'Callaghan, M. Lynch, V. Weldon, L. P. Barry, and J. F. Donegan, "Two-section singlemode lasers based on slots suitable for photonic integration," Electron. Lett. **48**(15), 945 (2012).
31. W.-H. Guo, Q. Lu, M. Nawrocka, A. Abdullaev, J. O'Callaghan, M. Lynch, V. Weldon, and J. F. Donegan, "Integrable Slotted Single-Mode Lasers," IEEE Photonics Technol. Lett. **24**(8), 634–636 (2012).
32. W.-H. Guo, Q. Lu, M. Nawrocka, A. Abdullaev, J. O'Callaghan, and J. F. Donegan, "Nine-channel wavelength tunable single mode laser array based on slots," Opt. Express **21**(8), 10215 (2013).

134.226.92.123 {ts '2021-09-28 09:31:20'}